"Sandwich"-like hybrid ZnO thin films produced by a combination of atomic layer deposition (ALD) and wet-chemistry using a mercapto silane as single organic precursor

Maria Kolympadi Markovic,[1,2] Robert Peter,[1,2] Ivana Jelovica Badovinac,[1,2] Iva Saric,[1,2] Marko Perčić,[2,3] Rafaela Radičić,[1] Dean Marković,[4] Mato Knez[5,6] and Gabriela Ambrožić*[1,2]

[1] University of Rijeka, Department of Physics, Radmile Matejčić 2, 51000 Rijeka, Croatia
[2] University of Rijeka, Centre for Micro- and Nanosciences and Technologies, Radmile Matejčić 2, 51000 Rijeka, Croatia
[3] University of Rijeka, Faculty of Engineering, Vukovarska 58, 51000 Rijeka, Croatia
[4] University of Rijeka, Department of Biotechnology, Radmile Matejčić 2, 51000 Rijeka, Croatia
[5] CIC nanoGUNE, 20018 San Sebastian, Spain
[6] IKERBASQUE, Basque Foundation for Science, 48013 Bilbao, Spain

E-mail: gabriela.ambrozic@uniri.hr

Received xxxxxx
Accepted for publication xxxxxx
Published xxxxxx

Abstract

This study describes a straightforward preparation of organic-inorganic thin films containing a stable "sandwich"-like structure of two atomic layer deposited (ALD) ZnO layers separated by a thin organosilane phase, which is built from a single organic component (3-mercaptopropyl)trimethoxysilane (MPTMS). Grafting of MPTMS on the first ALD ZnO layer was performed in solution and driven by the strong affinity of the terminal thiol functionality (-SH) towards ZnO. We demonstrate that under different reaction conditions, either MPTMS monolayers are prepared or a 5 nm thick cross-linked polymeric network is formed due to the self-condensation of silane, which covers the ALD ZnO surface. This film served as a soft template for the nucleation of an ALD ZnO top layer by creation of S-Zn and Si-O-Zn bonds at the upper interface, as confirmed by XPS measurements. An increase in surface roughness, as compared to the initial ZnO film, is observed after removal of the organic layer from the hybrid structure by calcination, which is accompanied by an improvement in UVA photocatalytic activity towards the degradation of methyl orange dye. Thus, MPTMS can be used as a sacrificial agent in combination with low temperature ALD processes for building rougher and photocatalytically efficient ZnO coatings.

Keywords: Atomic layer deposition, ZnO, hybrid thin films, organosilane, S-Zn bond, photocatalysis.

1. Introduction

Atomic layer deposition (ALD) is an automated technique for the growth of inorganic thin films that has several key advantages over other coating methods to meet today's technological needs for the fabrication of functional materials. [1] These advantages are excellent thickness control on the nanoscale and conformity to the substrate's structure, [2,3] but also relatively low processing temperatures which are compatible with any type of substrate, inorganic or organic, containing reactive surface groups. Related to ALD,

molecular layer deposition (MLD) can be used for the preparation of unique organic-inorganic hybrid films by applying organic gas precursors on inorganic substrates or alternating pulses of organic and organometallic precursors. [4-6] However, the application of organic precursors in MLD is restricted to volatile organic molecules with a high thermal stability under vacuum processing conditions. In order to grow a thicker organic phase by MLD on a solid substrate, numerous deposition cycles are required; therefore, a bifunctional precursor, or two or more organic precursors have to be selected. Studying different surface functional groups and their reactions with gas phase organic or organometallic precursors is crucial for expanding the scope of these processes. [7,8]

As an important semiconductor, ZnO has been intensely investigated using various ALD processes for its potential application in electronics, solar-energy devices, and catalysis, especially as photocatalyst for environmental remediation. [9-11] Moreover, several MLD depositions of zincone (Zn-O-R-O)$_n$ hybrid thin films have been reported by sequential pulsing of aliphatic or aromatic diols (OH-R-OH) and DEZ (diethyl zinc, Et_2Zn), [12-15] or by sub-saturated plasma-enhanced ALD (PE-ALD). [16] It is also known that similar MLD-deposited organic-inorganic hybrid films, for example Ti-containing hybrid films known as titanicones, [6] can be further used to produce nanoporous TiO_2 with enhanced photocatalytic activity, as compared to ALD TiO_2 films, obtained after removal of the organic components from the hybrid. [17] Contrary to titanicones and their resulting stable porous TiO_2 structures, the ambient instability and degradation of zincone thin films [14,15] represent serious issues in post-deposition applications of zinc-based hybrids, for example, in photocatalysis. [18] Taken into account that ZnO thin films or surface immobilized nanostructures are advantageous over dispersible photocatalytic materials due to their immediate reuse without additional separation steps in the wastewater treatment process, [19] alternative and simpler routes towards stable ZnO/hybrid nanofilms, which can be further processed for photocatalytic applications, are desirable.

Common trialkoxy organosilanes are one of the most applied reagents for solution-based surface chemical modifications of metal oxides. In dependence on the applied reaction conditions, one can obtain either covalently attached monolayers, or 3-D siloxanes grafted to the surface of metal oxides. Therefore, the tendency of silanes to perform hydrolytic self-condensation and form random or self-assembled structures through extending Si-O-Si bonding can be exploited for the formation of organic layers with different thicknesses. [20]

In the present contribution, we demonstrate a straightforward and simple approach to produce stable "sandwich"-like organic-inorganic hybrid thin films by combining ALD processing with traditional solution phase silanization. Our three-step procedure illustrated in Scheme 1, consists of: a) initial thermal ALD deposition of ZnO thin-films, b) ZnO surface modification with a few-nanometer thick polysiloxane network by applying only one organic precursor, and c) introduction of a second thin layer of ZnO by low-temperature ALD. The preparation of the intermediate organosilane layer relies on using a single organic precursor, (3-mercaptopropyl)trimethoxysilane (MPTMS). Being a common surface reagent frequently used for anticorrosive coatings, MPTMS is herein chosen for its bifunctional reactivity towards ZnO surfaces. [21-24] Namely, the mercapto functionality in MPTMS has a high binding affinity towards zinc ions in ZnO because of the formation of strong Zn-S bonds, as it was shown in previous studies using various thiol molecules and ZnO. [25-32] However, to our knowledge, the growth of ZnO films on substrates containing thiol groups has been rarely investigated. [31,32] On the other side, the silane end group of MPTMS, besides forming covalent bonds with hydroxyl groups present on surface, is also responsible for building interconnected polymeric structures through silane condensation/hydrolysis reactions. The tendency of MPTMS for self-polymerization has been previously exploited in advanced applications. [33-36] In this way we assure stable bilateral covalent attachments of the intermediate organic layer to both ZnO surfaces in the sandwich structure. The removal of the organic part by thermal calcination of the layered nanofilm resulted in an increase in surface roughness compared to the initial ALD ZnO film surface.

In order to elucidate the composition and surface-morphological properties of both hybrid and ceramic films, each of the samples, prepared in individual steps of a multistep treatment, was subjected to various experiments and investigated in detail. We show that the modification of the ZnO thin film surface improved their UVA photocatalytic activitiy towards the degradation of methyl orange (MO) and correlated the activity with the roughness and surface chemical composition by using a combination of characterization techniques: X-ray Photoelectron Spectroscopy (XPS), Scanning Electron Microscopy (SEM), Atomic Force Microscopy (AFM) and Secondary Ion Mass Spectrometry (SIMS). Moreover, we studied the effect of the applied reaction conditions on the monolayer formation and binding modes of MPTMS on the ALD ZnO surface, as well as the interfacial connection binding to the top ZnO layer in the hybrid structure.

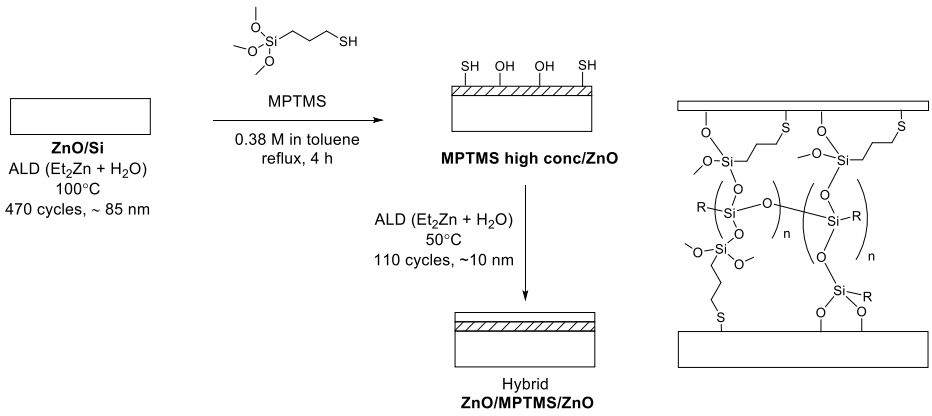

Scheme 1: Schematic representation of the preparation of "sandwich"-like ZnO-organosilane-ZnO hybrid thin films.

2. Methods

2.1 Materials

Single side polished, n-type, Si (100) wafers were cut in dimensions of 0.7×0.7 cm^2. Prior to ALD, they were cleaned with acetone, isopropanol and absolute ethanol (analytical grade solvents) in an ultrasound bath and dried under a stream of Ar. Diethylzinc, Et_2Zn (Strem Chemicals) and deionized water were employed as ALD precursors. N_2 (99.9999%) was used as carrier and purging gas. (3-Mercaptopropyl)trimethoxysilane, MPTMS (95%, Aldrich), toluene (anhydrous, max. 50 ppm H_2O, ≥99.8%, VWR chemicals), and methyl orange, MO (Kemika, Croatia) were employed as received.

2.2 Atomic Layer Deposition (ALD) processes

Depositions of ZnO thin films were carried out in a Beneq TFS-200 ALD system. The precursors were kept at 20 °C. The first ZnO layer with a thickness of ~85 nm (as measured by cross-sectional SEM images) was deposited at 100 °C on clean Si substrates applying 470 cycles consisting of the following sequence: Et_2Zn pulsing (200 ms), N_2 purging (1 s), water pulsing (180 ms), N_2 purging (1 s). These films are referred to as **ZnO/Si**. A second ZnO layer at 50 °C was deposited with 110 ALD cycles after the surface modification of first ZnO layer with a high concentration MPTMS in solution (*see* below), following the sequence indicated above. This time the ALD process started with water pulsing in order to hydrolyze potential Si-OMe groups exposed on the surface. The resulting hybrid materials are referred to as **ZnO/MPTMS/ZnO**.

A reference material, **Annealed ZnO bilayer**, was produced by applying the two previously described ALD processes (470 cycles at 100 °C, then 110 cycles at 50 °C), followed by post-deposition annealing in air at 600°C for 1 h in a preheated tube furnace. The resulting material was let to reach room temperature inside a desiccator.

2.3 Surface modification with MPTMS and calcination of hybrid structures

Preparation of silanized ZnO thin films from a higher concentration of MPTMS (sample **MPTMS high conc/ZnO**): In a round-bottomed flask, equipped with magnetic stirrer and condenser, 3 ZnO/Si substrates were added to toluene (10 mL) under Ar atmosphere and immediately after the ALD synthesis. To this very gently stirred mixture, MPTMS (0.800 mL, 4.09 mmol, final concentration 0.38 M) was added and the reaction mixture was heated under reflux for 4 h without stirring. Then, the substrates were washed several times with clean toluene and dried in an oven at 100 °C for 10 min.

Preparation of "sandwich"-like hybrid thin films **ZnO/MPTMS/ZnO** was performed by using **MPTMS high conc/ZnO** immediately after their preparation as substrates for ALD deposition of a second ZnO layer (*see* above).

The removal of the organic part of **ZnO/MPTMS/ZnO** was performed by thermal treatment in air at 600 °C for 1 h in a preheated tube furnace. The final materials were let to reach room temperature inside a desiccator and are referred to as **Calc ZnO/MPTMS/ZnO**. For comparison, some samples without the top ZnO layer were calcined under the same conditions to provide **Calc MPTMS high conc/ZnO** samples.

Preparation of silanized ZnO thin films from a lower concentration of MPTMS (sample **MPTMS low conc/ZnO**): 3 substrates **ZnO/Si** were immersed in a solution (10 mL) of MPTMS in toluene (concentration 3.8 x 10^{-3} M) and kept at room temperature and Ar atmosphere for 4 h. Then, they were

washed and dried as described for **MPTMS high conc/ZnO**. All samples were kept in a desiccator under vacuum until analysis.

2.4 Characterization techniques

Photoemission spectra were measured using a SPECS instrument equipped with a monochromatized source of Al Kα X-rays of 1486.74 eV and a hemispherical electron analyzer (Phoibos MCD 100). C 1s spectra were recorded with a pass energy of 10 eV, while S 2p and Si 2p spectra were taken with a pass energy of 20 eV. During XPS analysis, a typical pressure in the range of 10^{-7} Pa was maintained in the UHV chamber. Unifit software [37] was utilized to analyze the peaks, which were simulated with several sets of mixed Gaussian-Lorentzian functions, while the background was subtracted following Shirley's method. [38] In the S 2p spectra, each component was fitted as a $2p_{1/2}$ and $2p_{3/2}$ doublet with a spin-orbit splitting value of 1.2 eV and peak ratio area of 1:2. All spectra were calibrated by setting the C 1s peak to the binding energy (BE) of 284.5 eV.

SEM images were acquired using a Jeol JSM-7800F SEM instrument. A gentle beam mode was applied with an electron beam acceleration voltage of 0.7 kV at the working distance (WD) of 2 mm for the study of the surface morphology. The cross-sectional SEM images were obtained using 10 kV acceleration voltage at a WD of 4 mm and collecting backscattered electrons.

The surface topology scans of the analyzed samples were obtained by AFM using the Bruker Dimension Icon system. The tapping mode was used in order to obtain a high-resolution scan of the surface by using a Bruker SNL-10 type A silicon nitride cantilever with a silicon tip with 2 nm tip radius. The cantilever's dynamic properties, such as natural frequency and normal stiffness, were obtained by using the thermal tune method, for which the thermal noise spectra of the cantilever were measured and fitted to a Lorentzian harmonic oscillator model in air. The obtained calibration allows the use of minimal contact force for tapping for the measurement to have minimal impact on the surface. Scans of 1 μm^2 were acquired with 256 scan lines, each of them having 256 data points.

Elemental depth profiling was conducted by a Hiden SIMS Workstation, using 5 keV Cs^+ primary ions at the impact angle of 45° and collecting negative secondary ions. The depth of the SIMS crater was measured with a DEKTAK profiler.

2.5 Photocatalytic activity measurements

For the photocatalytic experiments, an aqueous solution of methyl orange (MO) dye in deionized water with a concentration of 8.0×10^{-6} M (2.6 ppm) was prepared. In each quartz Suprasil cuvette of the same series, the MO solution (2.5 mL) and a ZnO substrate were placed. A control experiment without the sample in MO solution was also conducted. The cuvettes were closed with quartz slides, kept in the dark for 30 min, and then from the top exposed to UVA irradiation inside a curing system Intelli-Ray 600 (Unitron International), equipped with a metal halide type arc lamp and a filter glass (for wavelengths < 315 nm). The substrates were placed at 13 cm distance from the lamp, resulting in an estimated irradiance of ~100 mW/cm^2. At certain intervals, absorption spectra of the upper solution were measured with a UV/Vis spectrometer Cary 60 (Agilent Technologies). The peak maximum at approximately 460 nm was used for monitoring the concentration of MO. According to the Lambert-Beer law, C_t/C_o, where C_t is the concentration at the corresponding time interval and C_o the initial concentration, is equal to the measured UV absorption value A_t/A_o. The prepared MO solution had a pH value of 6.8, which remained unchanged during the experiments until it became colorless.

3. Results and Discussion

3.1 Surface modification of ALD ZnO thin films with MPTMS in solution

ZnO thin films with ~85 nm thickness were grown on Si wafers by thermal ALD at 100 °C (**ZnO/Si**) and used for subsequent surface chemical modification under two different conditions: a) immersion in a 3.8 x 10^{-3} M solution of MPTMS in toluene at room temperature (sample **MPTMS low conc/ZnO**), and b) reflux of a 0.38 M solution of MPTMS in toluene (sample **MPTMS high conc/ZnO**). In both cases, XPS measurements revealed the appearance of new peaks attributed to S 2p and Si 2p atomic states, confirming the binding of MPTMS molecules to ALD ZnO films. As discussed below, conclusions are drawn regarding the formation of a monolayer or multilayers under first and second applied reaction conditions, respectively. The absolute intensities of the XPS peaks reflect the concentration differences of MPTMS used in the two solutions and are accompanied by a corresponding decrease in the Zn 2p peak intensities (Figure S1 in Supplementary Data). The Si 2p peak region is discussed in detail in Figure 5 (Section 3.2). Moreover, the C 1s regions of both silane-modified surfaces are deconvoluted into 3 components, C-C/C-Si, C-S, and C-O, due to the presence of intact Si-O-Me groups (Figure S2 in Supplementary Data). [21,24]

Figure 1 presents normalized Zn $2p_{3/2}$, O 1s, and S 2p XPS plots of the **MPTMS low conc/ZnO** and **MPTMS high conc/ZnO** samples compared to **ZnO/Si**. The O 1s regions

mainly consist of two contributions: a peak at the BE of 530.2 eV, attributed to oxygen bound in the ZnO lattice, and a peak at approximately 532 eV, resulting from all oxygen-containing species that are chemi- or physisorbed on the surface. [39] Compared to the initial substrate, a greater increase of the O 1s component, ascribed to the surface-adsorbed oxygen species attributed to the newly formed bonds (i.e. Si-O-Zn, Si-O-Si, Si-OH, Si-O-C, and perhaps trapped H_2O), is observed for **MPTMS high conc/ZnO**, reflecting the higher amount of the bound silane (Figure 1(c)). Additionally, the Zn 2p peaks of **MPTMS high conc/ZnO** were unsymmetrical with a broadening towards higher BEs. A peak deconvolution of Zn $2p_{3/2}$ revealed a new component at 1022.8 eV apart from the original signal of Zn^{2+} in the ZnO lattice at 1021.7 eV. Dissociative adsorption of thiol as thiolate on the ZnO surface [26] and adsorption of hydrogen atoms split from the S-H group can produce $Zn(OH)_2$, which in previous reports was assigned to Zn $2p_{3/2}$ peaks at 1022.7-1021.8 eV. [39,40] We therefore examined the Auger Zn lines at around 500 eV, but they were very similar to the initial **ZnO/Si** substrate, meaning that there is no significant increase in hydroxylated surface species. Another possible explanation is that a high content of sulfur-containing molecules may alter the chemical environment or oxidation state of some Zn ions close to the surface that can lead to peak broadening. O^{2-} ions at the ZnO surface may diffuse and undergo replacement by sulfur. A recent study on ZnO nanoparticles showed that such sulfur/oxygen diffusion may lead to partial formation of an external ZnS shell covering the ZnO core. [41] Moreover, zincoxysulfide Zn(O,S) alloys and mixed phases have been reported to exhibit a shift of the Zn 2p peaks towards higher BEs. [42,43] In contrast to the samples modified with a high concentration of the silane reagent, the Zn 2p peaks of **MPTMS low conc/ZnO** do not show any broadening (Figure 1(b)), which also suggests that the sulfur/oxygen exchange depends on the sulfur content on the surface according to the proposed mechanism of sulfidation of ZnO nanoparticles. [44]

For **MPTMS low conc/ZnO** (Figure 1(b)), the S 2p core level spectrum was fit into two components, centered at 162.3 and 163.5 eV, considering the spin-orbit splitting for each contribution. These components are attributed to thiolate species in S-Zn bonds and thiol S-H bonds with relative concentrations of 90% and 10%, respectively. No oxidized sulfur molecules were detected. In this case the surface modification is dominated by the formation of S-Zn bonds indicating the major presence of monolayers. This result is in agreement with experiments conducted by Whitten and Steeves in the gas phase under ultrahigh vacuum of the XPS instrument and room temperature, which produced only species bound through S-Zn bonds, even after intentional addition of H_2O vapors. [24]

The numerical fitting of the S 2p core level spectrum of **MPTMS high conc/ZnO** (Figure 1(c)) exhibited 50% thiolate S-Zn bonds, 39% S-H bonds and 11% oxidized SO_x species (sulfinates and sulfonates) at 168.5 eV. Petoral, Jr and co-workers have reported similar ratios for the functionalization of ZnO films prepared by plasma-assisted molecular beam epitaxy with vaporized MPTMS. [22] They suggested the formation of silane monolayers bound via Zn-S bonds, and silanoxy groups which result in free thiol groups. In a more recent article, Uvdal and co-workers mentioned the binding of MPTMS exclusively *via* the silane moiety to annealed ZnO thin films when treated with the silane solution in xylene at room temperature. [23] In our case, we conclude that MPTMS is connected to the surface mainly through thiolate S-Zn bonds, similar to the low concentration case of MPTMS, while the increased amount of free thiol S-H results upon self-condensation of the reagent, which is favored at high temperatures and concentrations of the reagent. [34] Additional evidence of the predominant binding of MPTMS on ZnO *via* SH groups was provided by the XPS Si 2p core level spectrum presenting a low content of silane binding Si-O-Zn (*see* Section 3.2 and Figure 5).

If compared with the images of the initial **ZnO/Si** (Figure 2(a)), the **SEM** micrographs of **MPTMS high conc/ZnO**, shown in Figure 2(b) indeed confirmed the presence of an inter-linked polymerized network which covered the whole surface of the inorganic material. Consequently, a significant increase in surface roughness was measured by AFM, with the root mean square (rms) value increasing from 1.2 nm (**ZnO/Si**) to 7.8 nm (**MPTMS high conc/ZnO**). From the cross-sectional SEM images, the thickness of the organic film of the sandwich hybrid **ZnO/MPTMS/ZnO** structures, that are described in Section 3.2, is estimated to be 5 nm on average. The formation of multilayer polymer structures, like those proposed for the functionalization of SiO_2 nanoparticles, can be envisaged. [34]

It is also worth mentioning that the synthesis of **MPTMS high conc/ZnO** was reproducible in terms of surface morphology observed by SEM, XPS peak intensities and S-H/S-Zn peak ratios. The hydrolytic self-condensation of silane molecules in solution can be avoided at low temperatures and concentrations of the reagent as shown in the case of **MPTMS low conc/ZnO**. The tendency of silanes to create higher order structures can be exploited for the alteration of the initial morphology of the ALD ZnO surfaces simply by changing the conditions of the surface functionalization reaction in solution. The exposed free thiol -SH groups, along with silanol Si-OH groups produced by the easily hydrolyzed alkoxy silane moieties in **MPTMS high conc/ZnO**, can serve as nucleation sites for the deposition of a top ZnO layer by ALD.

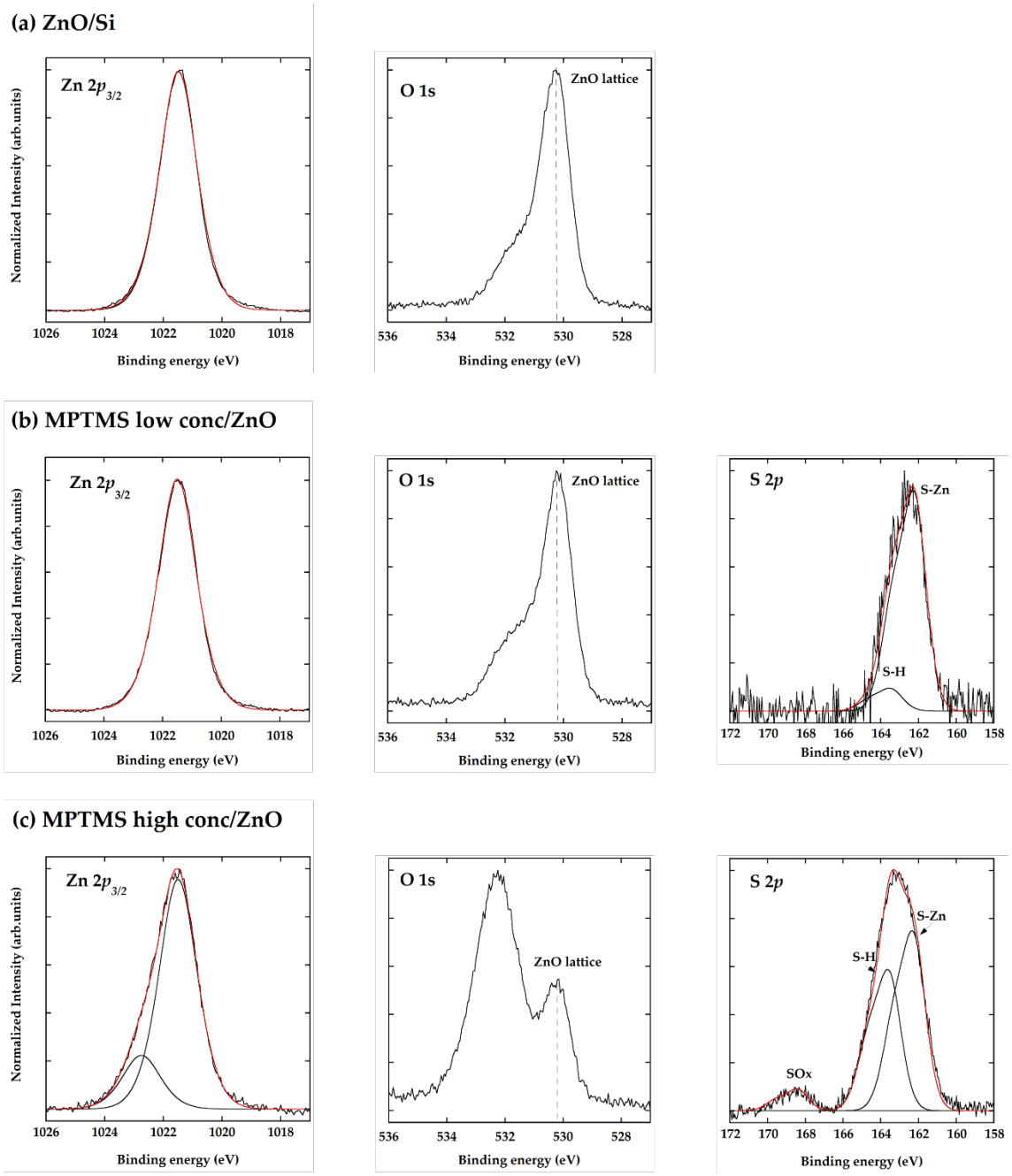

Figure 1: (a) XPS Zn 2p3/2 and O 1s core level spectra of unmodified ALD ZnO thin films (**ZnO/Si**); (b) and (c) Zn 2p3/2, O 1s and S 2p core level spectra of MPTMS-modified ZnO thin films with low and high concentration of organosilane, **MPTMS low conc/ZnO** and **MPTMS high conc/ZnO**, respectively. Red lines represent the numerical fit of the measured peaks.

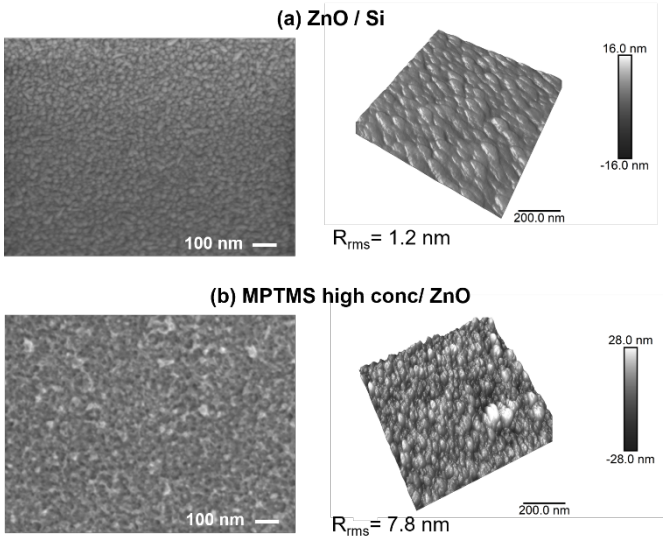

Figure 2. SEM images (left) and tapping mode AFM images (right) showing the surface morphology of: (a) **ZnO/Si** (470 cycles, 100 °C), (b) **MPTMS high conc/ZnO** (0.38 M in refluxing toluene).

3.2 Preparation of hybrid ZnO-organosilane-ZnO thin films and their calcination

A ZnO layer was deposited on top of **MPTMS high conc/ZnO** with 110 ALD cycles, in order to create a "sandwich"-like structure, **ZnO/MPTMS/ZnO**. A lower deposition temperature (50 °C) was applied in this process in order to minimize the thermal impact on the cross-linked polymer. [45,46] The SEM images of the hybrid in Figure 3(a) (top right) show a complete coverage of the MPTMS polymer, on which the ZnO crystallites form a continuous and conformal ZnO film. The inset shows a SEM cross-section, where the contrast between the darker organic film in the middle and the brighter ZnO edge layers is visible, confirming the layered structure. From the high magnification cross-sectional SEM images of the hybrid film, we estimated the average thickness of the ALD-deposited ZnO layer to be approximately 10 nm (Figure 3(a) (bottom)).

Additionally, we performed elemental depth profiles for ZnO, S and Si of the hybrid **ZnO/MPTMS/ZnO** by SIMS. The ZnO signal is characterized by two steps: the first step corresponds to the top ZnO layer, and the second step to bottom ZnO layer (Figure 3(a) (top left)). At this point it should be emphasized that the thickness of the top ZnO layer, as measured by SIMS, is lower than the actual value assessed by SEM. The reason is that SIMS depth analysis could not be used for accurate thickness determination of the thin top ZnO layer film, since the equilibrium between sputtering and implantation of primary ions (Cs^+) in the sample is reached only after few nanometers beneath the surface. [47] Nevertheless, the SIMS profile of the interspace region between two ZnO layers shows intense S and Si signals, indicating the presence of a distinct MPTMS organosilane phase, thus confirming the sandwich structure of **ZnO/MPTMS/ZnO**. It should be noted that primary ions cause some mixing of ZnO and MPTMS phases, [47] and an overlap of these two phases may result in less defined interfaces.

Furthermore, an increase in the intensity of the O 1s component region in XPS, which is attributed to the ZnO lattice at 530.2 eV, shown in Figure 4(a), as well as an increase in intensity of the Zn 2p peaks (not shown), proved the deposition of a ZnO layer on top of **MPTMS high conc/ZnO** (*see* Figure 1(c)). The component attributed to different oxygenated bonds appears now less broad than in the starting material, either because some species cannot be detected from the lower interface between MPTMS and ZnO or exposed Si-OH groups have reacted with Et_2Zn during the deposition of the top ZnO layer, as explained below.

Additionally, S 2p and Si 2p signals were detected, but with a low intensity, likely because the intermediate organic film is buried under the top ZnO layer and therefore close to the depth limitations of XPS photoelectrons. Nevertheless, these signals revealed valuable information about the organic-inorganic interface created during the second ALD process. In the S 2p core spectrum (Figure 4(a)), apart from some oxidized sulfur species SOx, only the component centered at 162.3 eV was observed which can be assigned to S-Zn bonds. This is an evidence that exposed -SH groups of the polymeric MPTMS film are reacting with Et_2Zn vapors during the initial ALD cycles. Although Zn has a high affinity to thiols, to our knowledge, only two previous study reported the growth of ZnO continuous thin films on surface thiol groups. [31, 32]

The above results can be combined with the XPS spectra of the Si 2p region shown in Figure 5. The Si 2p core-level spectrum of **ZnO/MPTMS/ZnO** reveals an additional component with a BE at 101.1 eV, which is lower than the symmetric Si 2p peak at 102.2 eV (including mainly Si-O-C, Si-C, Si-O-H, Si-O-Si, and low content of Si-O-Zn species) of the polymer substrate **MPTMS high conc/ZnO** (Figure 5(a) and (b)). This new component can be attributed to Si-O-Zn bonds with an attached top ZnO layer. [48] In this way, we conclude that Et_2Zn binds to the exposed free -SH and -OH groups of the interconnected organosilane polymer structure *via* the formation of strong covalent S-Zn and Si-O-Zn bonds. These hybrid materials were found to be stable in air since their XPS spectra remained unchanged even after two months.

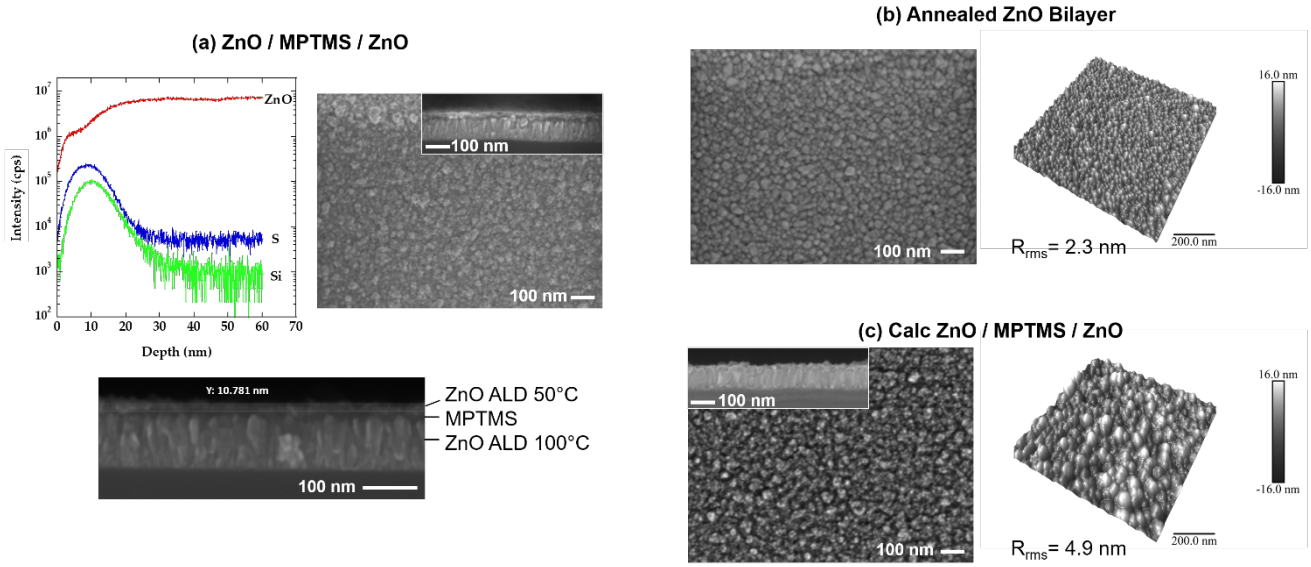

Figure 3. (a) SIMS elemental depth profiles (top left) for ZnO, S and Si, the corresponding SEM top-view image (top right) of **ZnO/MPTMS/ZnO** sandwich structure with a SEM cross-section inset, and higher magnification of this SEM cross-section (bottom) indicating the thickness of the upper ZnO layer (110 cycles, 50°C); (b) SEM top-view image (left), and tapping mode AFM image (right) of **Annealed ZnO Bilayer**; (c) SEM top-view image (left) with a SEM cross-section inset, and tapping mode AFM images (right) of **Calc ZnO/MPTMS/ZnO** (calcination at 600 °C in air).

Next, the hybrid materials were calcined at 600 °C in air in order to completely remove the organic component. SEM and AFM images in Figure 3(c) show a granular surface morphology of the final **Calc ZnO/MPTMS/ZnO**. The inset cross-sectional SEM image showes small grains on the top surface, while the bulky part shows coalesced ZnO columns.

In order to assess the templating effect of the organic interface on the surface morphology of ZnO in **Calc ZnO/MPTMS/ZnO**, we prepared a reference material (**Annealed ZnO Bilayer)** as follows: initial deposition of ZnO on **ZnO/Si** under the same low-temperature ALD processing conditions applied for depositing the top ZnO layer in **ZnO/MPTMS/ZnO** (110 cycles at 50 °C), followed by a thermal treatment at 600 °C in air. The top-view SEM image of the resulting ZnO film is shown in Figure 3(b). When compared to **Calc ZnO/MPTMS/ZnO**, the surface of the material in absence of the organic layer consisted of ZnO nanocrystals, compact and equal in size,which are formed by a coalescence of smaller grains due to Ostwald ripening during the thermal annealing. [49] A roughness rms value of 2.3 nm was measured by AFM. On the other side, the coalescence effect was much less pronounced in **Calc ZnO/MPTMS/ZnO** (top-view SEM image in Figure 3(c)), where the sacrificial organosilica layer acted as a soft polymer template controlling the coalescence process. Namely, silane molecules act as barriers between the ZnO seeds by inhibiting their aggregation, possibly in a similar way as in modified metal oxide nanoparticles. [25] Moreover, strong binding with the polymer substrate may have induced the localized growth of ZnO seeds. Regions of ~40-50 nm, consisting of ZnO crystallites (~10 nm or less), with obvious gaps in between, are visible. In comparison with the initial **ZnO/Si** (AFM image shown in Figure 2(a)), more pinholes can be observed and the rms roughness value of the surface increased from 1.2 nm (**ZnO/Si**) to 4.9 nm (**Calc ZnO/MPTMS/ZnO**).

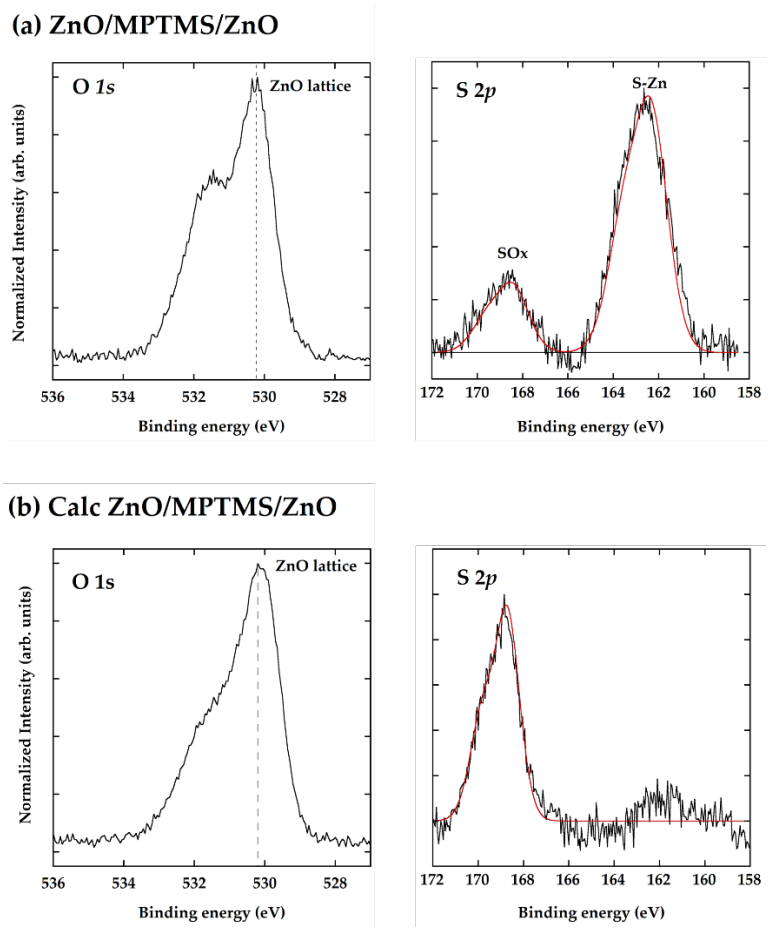

Figure 4: XPS O 1s and S 2p core level spectra of: (a) **ZnO/MPTMS/ZnO**, and (b) **Calc ZnO/MPTMS/ZnO**. Red lines represent the numerical fit of the measured peaks.

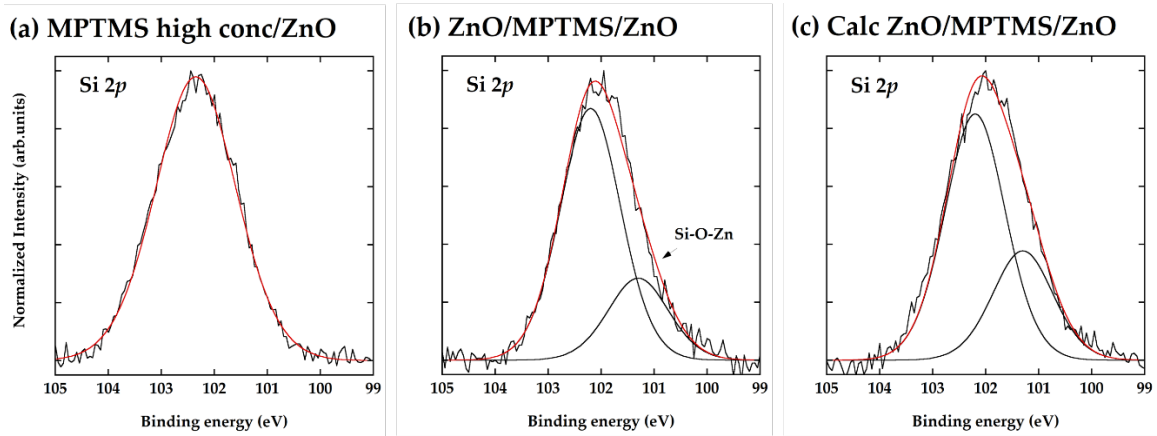

Figure 5: XPS Si 2p core level spectra of: (a) **MPTMS high conc/ZnO**, (b) **ZnO/MPTMS/ZnO**, and (c) **Calc ZnO/MPTMS/ZnO**. Red lines represent the numerical fit of the measured peaks.

After calcination, the C 1s XPS peak of **Calc ZnO/MPTMS/ZnO** confirmed the drastic decrease in carbon content, apart from some carbon contamination due to exposure of the samples to ambient conditions (not shown). In the S 2p region (Figure 4(b)), the S-Zn peak disappeared as S-Zn bonds are expected to be stable only up to approximately 400 °C. [27] Only a very low intensity peak at around 168 eV corresponding to oxidized sulfur species, can be detected, possibly because of entrapment of volatile sulfur compounds derived from the lower layer. [50] Alterations in O 1s XPS regions can be observed between the initial **ZnO/Si** (Figure 1(a)) and the final **Calc ZnO/MPTMS/ZnO** (Figure 4(b)). The fraction of oxygenated species attached to the ZnO surface is increased after deposition of the second ALD ZnO layer and calcination, indicating an overall increase of oxygenating species, including zinc hydroxylated species. The Si 2p signal (Figure 5(c**)**) exhibits the same pattern as the hybrid **ZnO/MPTMS/ZnO**. These silicon species can be ascribed to regions with extended Si-O-Si cores and zinc silicates as remains of MPTMS that cannot be removed during the thermal heating. [51,52] In total, traces of sulfur and silicon in the range of 0.5-1 % can be detected by XPS on the surface of the final structure.

In order to assess the role of the Si contamination that cannot be removed from the material by thermal treatment, and to identify potential surface etching events of ZnO during calcination, we examined the surface morphology and composition of the modified films by calcining the **MPTMS high conc/ZnO** films under the same conditions (600 °C in air) as for the sandwich structures, but without the deposition of the top ZnO layer. Top-view SEM and AFM images and XPS Si 2p measurements are shown in Figure S3 (Supplementary Data). It should be noted that no S species could be detected by XPS. The rms surface roughness value increased from 1.2 nm (**ZnO/Si**) to 3.2 nm (**Calc MPTMS high conc/ZnO**). Although some obvious pits are observed in the SEM images, which cannot exclude a small degree of surface etching by the thiol, [28,29] the increase in roughness is mostly owned to the high content of oxidized Si species on the surface. [51] This was confirmed with the XPS Si 2p peak at 103.2 eV and estimated to amount to 20 % of the surface entities.

3.3 Evaluation of photocatalytic properties

To understand the relationship between the photocatalytic activities of ALD ZnO thin films [40,45,53, 54] and the degree of surface chemical functionalization by MPTMS or their increased roughness after the thermal removal of the organic template, two sets of experiments were conducted on both hybrid and ceramic films by monitoring the photodegradation of an aqueous solution of methyl orange (MO) (Figure 6). Before being exposed to UVA light, the analyzed mixtures were kept in the dark for 30 min in order to establish an adsorption-desorption equilibrium of the dye on the photocatalyst's surface, but without measuring significant changes in the concentration of the dye in solution. The photocatalytic reaction appears to follow zero order kinetics, [55] in other words the rate constants, k (given in Table 1) do not depend upon the initial concentration of MO in solution according to the integrated rate law: $C_t = C_o - kt$. This is a situation when the heterogeneous catalyst surface, where the reaction takes place, is saturated by the organic dye molecules and there are no limitations in photon supply.

Figure 6(a) illustrates the degradation curves of MO in presence of the hybrid materials, i.e. **MPTMS high conc/ZnO** and **MPTMS low conc/ZnO**. For comparison, the photocatalytic activity of **ZnO/Si** is presented as reference. The better performance of **MPTMS low conc/ZnO** versus **MPTMS high conc/ZnO** can be explained as follows: an increased amount of S-Zn bonds on the surface of the latter sample is responsible for surface passivation, thus blocking the oxygen vacancies which are considered responsible for photocatalysis. [24] On the other hand, surprisingly, a monolayer of thiol molecules on the ZnO surface bound via S-Zn bonds in **MPTMS low conc/ZnO** slightly elevates the photocatalytic activities when compared to the **ZnO/Si**. The reason for this phenomenon is unclear. However, the finding is consistent with a recent study which concluded that an optimal distribution of L-cysteine molecules bound to ZnO nanoparticles can induce the production of H_2O_2 molecules under light exposure. [56] This indicates that in our case probably incomplete monolayered domains are formed, which have a beneficial effect on the photocatalytic activity, without blocking active sites on the ZnO.

Among our ceramic films, **Calc ZnO/MPTMS/ZnO** showed the best photocatalytical performance with a 40% increase of the zero order constant rate when compared to the ZnO/Si reference (Figure 6(b)). This result is connected to the increased surface roughness, and thus the presence of more photoactive species as a consequence of the templating effect of sacrificial MPTMS polymer and the formation of small ZnO crystallites. In absence of any organic template, the thermally treated bilayer of ZnO **Annealed ZnO Bilayer** showed a lower photocatalytic activity when compared to then **ZnO/Si**, although a small increase of the roughness is measured in the former. Namely, ALD ZnO thin film were reported to exhibit lower photocatalytic activites after annealing at 500 or 600 °C in air due to the absence of defects and the improved film density. [49]

Moreover, the small remaining sulfur content in the final **Calc ZnO/MPTMS/ZnO** thin films may have a beneficial role on the increase of its catalytic activity as it is shown in other systems. [57] The presence of Si residues, remaining after

calcination of the organic interlayer at depths >10 nm, does not seem to interfere with the photocatalytic activity. However, a substantial amount of surface/subsurface oxidized Si species in **Calc MPTMS high conc/ZnO**, for which the top ALD ZnO layer was ommited, showed similar activities with **ZnO/Si** (overlapped photodegradation curves), contrasting the reports in which SiO_2 passivates photocatalytic processes [58].

Therefore, the poorer photocatalytic properties of **Calc MPTMS high conc**, **Annealed ZnO Bilayer/ZnO** and **ZnO/Si**, which are correlated with their lower surface roughness and surface contamination with SiOx species formed during the calcination process, indeed confirmed that the three step procedure for preparing **Calc ZnO/MPTMS/ZnO**, i.e. silanization of ALD ZnO layer, addition of a second ZnO layer, and calcination, was beneficial for generating ZnO with improved photocatalytic performance.

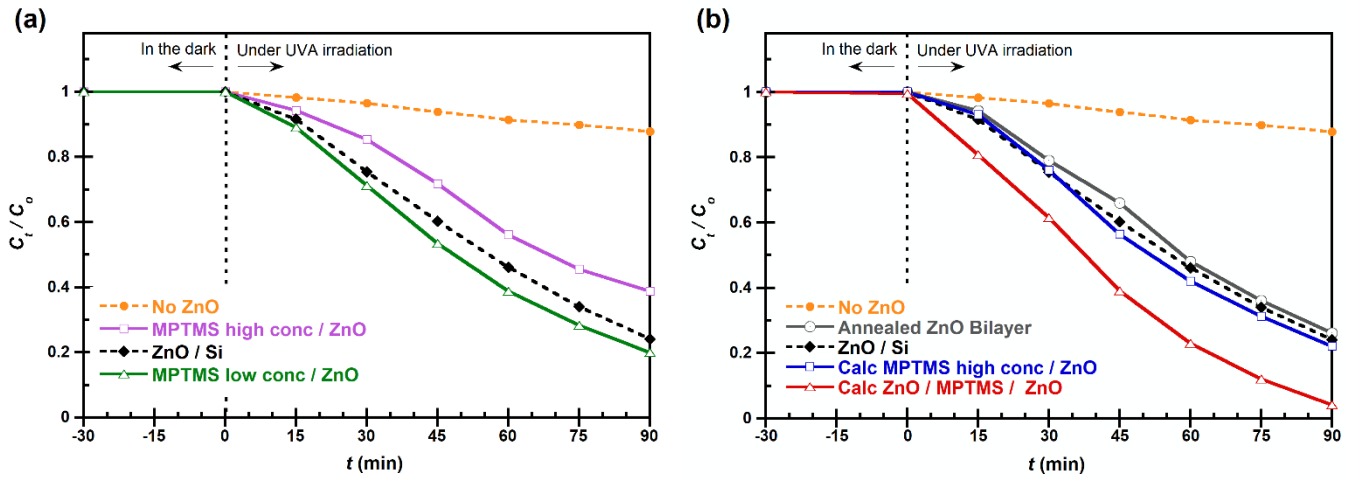

Figure 6: Photodegradation curves of methyl orange (MO) versus irradiation time in presence of: (a) **MPTMS low conc/ZnO** and **MPTMS high conc/ZnO**; (b) **Calc ZnO/MPTMS/ZnO**, **Calc MPTMS high conc/ZnO** and **Annealed ZnO Bilayer**. The initial **ZnO/Si** (470 ALD cycles, 100°C) was used as reference.

Table 1: Apparent zero order rate constants and the corresponding normalized values to the samples' surface area for the photodegradation of methyl orange (MO) as extracted from the linear fitting of the curves in Figure 6(a) and 6(b) up to 60 min of UVA light exposure.

	Samples	Zero order rate constant ($M\ min^{-1}$)	Zero order rate constant normalized to the surface area ($M\ min^{-1}\ cm^{-2}$)	R^2
Figure 6(a)	MPTMS high conc/ZnO	0.59×10^{-7}	1.20×10^{-7}	0.9655
	ZnO/Si	0.74×10^{-7}	1.52×10^{-7}	0.9914
	MPTMS low conc/ZnO	0.84×10^{-7}	1.72×10^{-7}	0.9945
Figure 6(b)	Annealed ZnO Bilayer	0.70×10^{-7}	1.44×10^{-7}	0.9764
	Calc MPTMS high conc/ZnO	0.83×10^{-7}	1.70×10^{-7}	0.9798
	Calc ZnO/MPTMS/ZnO	1.04×10^{-7}	2.12×10^{-7}	0.9982

4. Conclusions

In summary, a simple and straightforward approach using ZnO thin films, grown by ALD, and a common mercapto silane MPTMS, was demonstrated for the construction of inorganic-organosilane-inorganic layered structures via strong S-Zn and Si-O-Zn bonds. Under the described experimental conditions, MPTMS created a distinct cross-linked polymeric network on the ZnO film, which was used as a substrate to nucleate and grow a second ALD ZnO layer on the exposed thiol and silanol groups. The methodology utilizes one single component MPTMS to obtain a few nanometers thick organosilane phase between the two ZnO layers. These hybrid materials are stable in air, in contrast to previously reported zincones.

Thermal removal of the organosilane phase resulted in inhibition of a ZnO crystal growth on the surface and in the formation of thin films with an increased roughness. The template effect of self-polymerized MPTMS enhanced the roughness of a 10 nm thick ZnO upper layer, which improved the photocatalytic properties of the initial material by 40% in the zero-order reaction kinetics regime. Given that MPTMS is a common commercially available reagent for surface modification, our investigations show that it can be potentially used as sacrificial agent for the developement of rougher and more efficient photocatalytically active ZnO coatings in combination with ALD processes.

Acknowledgements

This work was mainly supported by the Croatian Science Foundation under project number IP-2016-06-3568, and in part by the University of Rijeka under project number 16.12.2.1.01. We also acknowledge financial support from the European Fund for Regional Development and the Ministry of Science, Education and Sports of the Republic of Croatia under the project Research Infrastructure for Campus based Laboratories at the University of Rijeka (grant number RC.2.2.06-0001) for the acquiring of instrumentation used in this work. Mato Knez acknowledges support by the Spanish Ministry of Economy and Competitiveness (MINECO) within grant agreement no. MAT2016-77393-R, including FEDER Funds.

References

[1] C. Sanchez, C. Boissiere, S. Cassaignon, C. Chaneac, O. Durupthy, M. Faustini, D. Grosso, C. Laberty-Robert, L. Nicole, D. Portehault, F. Ribot, L. Rozes C. Sassoye, Molecular Engineering of Functional Inorganic and Hybrid Materials, Chem. Mater. 26 (2014) 221-238.

[2] S. M. George, Atomic Layer Deposition: An Overview, Chem. Rev. 110 (2010) 111-131.

[3] A. S. Asundi, J. A. Raiford, S. F. Bent, Opportunities for Atomic Layer Deposition in Emerging Energy Technologies, ACS Energy Lett. 4 (2019) 908-925.

[4] P. Sundberg, M. Karppinen, Organic and inorganic–organic thin film structures by molecular layer deposition: A review, Beilstein J. Nanotechnol. 5 (2014) 1104-1136.

[5] K. Gregorczyk, M. Knez, Hybrid Nanomaterials through Molecular and Atomic Layer Deposition: Top, Down, Bottom up, and In-between Approaches to New Materials, Prog. Mater. Sci. 75 (2016) 1-37.

[6] X. Meng, An overview of molecular layer deposition for organic and organic–inorganic hybrid materials: mechanisms, growth characteristics, and promising applications, J. Mater. Chem. A 5 (2017) 18326-18378.

[7] R. Edy, G. Huang, Y. Zhao, Y. Guo, J. Zhang, Y. Mei, J. Shi, Influence of reactive surface groups on the deposition of oxides thin films by atomic layer deposition, Surf. Coat. Technol. 25 (2017) 149-154.

[8] F. Yang, J. Brede, H. Ablat, M. Abadia, L. Zhang, C. Rogero, S. D. Elliott, M. Knez, Reversible and Irreversible Reactions of Trimethylaluminum with Common Organic Functional Groups as a Model for Molecular Layer Deposition and Vapor Phase Infiltration, Adv. Mater. Interfaces 4 (2017) 1700237.

[9] C. Wöll, The Chemistry and Physics of Zinc Oxide Surfaces, Prog. Surf. Sci. 82 (2007) 55-120.

[10] T. Tynell, M. Karppinen, Atomic layer deposition of ZnO: a review, Semicond. Sci. Technol. 29 (2014) 043001.

[11] C. H. Burgess, Review of tailoring ZnO for optoelectronics through atomic layer deposition experimental variables, Mater. Sci. Tech. 33 (2016) 809-821.

[12] Q. Peng, B. Gong, R. M. VanGundy, G. N. Parsons, "Zincone" Zinc Oxide-Organic Hybrid Polymer Thin Films Formed by Molecular Layer Deposition, Chem. Mater. 21 (2009) 820-830.

[13] B. Yoon, B. H. Lee, S. M. George, Highly Conductive and Transparent Hybrid Organic-Inorganic Zincone Thin Films Using Atomic and Molecular Layer Deposition, J. Phys. Chem. C 116 (2012) 24784-24791.

[14] D. Choudhury, G. Rajaraman, S. K. Sarkar, Stability of molecular layer deposited zincone films: experimental and theoretical exploration, RSC Adv. 5 (2015) 29947-29952.

[15] A. Morteza, J.-P. Niemala, W. M. M. Kessels, M. Creatore, On the role of micro-porosity in affecting the

environmental stability of atomic/molecular layer deposited (ZnO)a(Zn-O-C6H4-O)b films, Dalton Trans. 48 (2019) 3496-3505.

[16] A. Perrotta, J. Pilz, S. Pachmajer, A. Milella, A. M. Coclite, On the transformation of "zincone"-like into porous ZnO thin films from sub-saturated plasma enhanced atomic layer deposition, Beilstein J. Nanotechnol. 10 (2019) 746-759.

[17] C. Chen, P. Li, G. Wang, Y. Yu, F. Duan, C. Chen, W. Song, Y. Qin, M. Knez, Nanoporous Nitrogen-Doped Titanium Dioxide with Excellent Photocatalytic Activity under Visible Light Irradiation Produced by Molecular Layer Deposition, Angew. Chem. Int. Ed. 52 (2013) 9196-9200.

[18] X. Liang, Y.-B. Jiang, A. W. Weimer, Nanocoating zinc alkoxide (zincone) hybrid polymer films on particles using a fluidized bed reactor, J. Val. Sci. Technol. A 30 (2012) 01A108.

[19] S. K. Loeb, P. J. J. Alvarez, J. A. Brame, E. L. Cates, W. Choi, J. Crittenden, D. D. Dionysiou, Q. Li, G. Li-Puma, X. Quan, D. L. Sedlak, T. D. Waite, P. Westerhoff, J.-H. Kim, The Technology Horizon for Photocatalytic Water Treatment: Sunrise or sunset?, Environ. Sci. Technol. 53 (2019) 2937-2947.

[20] L. Li, B. Li, J. Dong, J. Zhang, Roles of silanes and silicones in forming superhydrophobic and superoleophobic materials, J. Mater. Chem. A 4 (2016) 13677-13725.

[21] F. Sinapi, L. Forget, J. Delhalle, Z. Mekhalif, Self-assembly of (3-mercaptopropyl)trimethoxysilane on polycrystalline zinc substrates towards corrosion protection, Appl. Surf. Sci. 212-213 (2003) 464-471.

[22] R. M. Petoral, Jr., G. R. Yazdi, A. Lloyd Spetz, R. Yakimova, K. Uvdal, Organosilane-functionalized wide band gap semiconductor surfaces, Appl. Phys. Lett. (2007) 223904.

[23] L. SelegArd , V. Khranovskyy, F. Söderlind, C. Vahlberg , M. Ahrén, P.-O. Käll, R. Yakimova, K. Uvdal, Biotinylation of ZnO nanoparticles and thin films: A two-step surface functionalization study, ACS Appl. Mater. Interfaces 2 (2010) 2128-2135.

[24] J. Singh, J. Im, E. J. Watters, J. E. Whitten, J. W. Soares, D. M. Steeves, Thiol dosing of ZnO single crystals and nanorods: Surface chemistry and photoluminescence, Surf. Sci. 609 (2013) 183-189.

[25] N. S. Pesika, Z. Hu, K. J. Stebe, P. C. Searson, Quenching of Growth of ZnO Nanoparticles by Adsorption of Octanethiol, J. Phys. Chem. B 106 (2002) 6985-6990.

[26] B. Halevi, J. Vohs, Reactions of CH_3SH and $(CH_3)S_2$ on the (0001) and (000$\bar{1}$) Surfaces of ZnO, J. Phys. Chem. B 109 (2005) 23976-23982.

[27] P. W. Sadik, S. J. Pearton, D. P. Norton, E. Lambers, F. Ren, Functionalizing Zn- and O-terminated ZnO with thiols, J. Appl. Phys. 101 (2007) 104514.

[28] J. Chen, R. E. Ruther, Y. Tan, L. M. Bishop, R. J. Hamers, Molecular Adsorption on ZnO(1010) Single-Crystal Surfaces: Morphology and Charge Transfer, Langmuir 28 (2012) 10437-10445.

[29] J. Singh, J. Im, J. E. Whitten, J. W. Soares, D. M. Steeves, Encapsulation of Zinc Oxide Nanorods and Nanoparticles, Langmuir 25 (2009) 9947-9953.

[30] Y. Tong, T. Jiang, S. Qiu, K. Koshmak, A. Giglia, S. Kubsky, A. Bendounan, L. Chen, L. Pasquali, V. A. Esaulov, H. Hamoudi, ZnO Functionalization: Metal-Dithiol Superstructures on ZnO(0001) by Self-Assembly, J. Phys. Chem. C 122 (2018) 2880-2889.

[31] J. W. P. Hsu, W. M. Clift, L. N. Brewer, Zinc Oxide Growth Morphology on Self-Assembled Monolayer Modified Silver Surfaces, Langmuir 24 (2008) 5375-5381.

[32] G. Ambrožić, M. Kolympadi Markovic, R. Peter, I. Kavre Piltaver, I. Jelovica Badovinac, D. Čakara, D. Marković, M. Knez, Building organosilica hybrid nanohemispheres *via* thiol-ene click reaction on alumina thin films deposited by atomic layer deposition (ALD), J. Colloid Interface Sci. 560 (2020) 303-311.

[33] F. He, W. Wang, J.-W. Moon, J. Howe, E. M. Pierce, L. Liang, Rapid Removal of Hg(II) from Aqueous Solutions Using Thiol-Functionalized Zn-Doped Biomagnetite Particles, ACS Appl. Mater. Interfaces 4 (2012) 4373-4379.

[34] G. Mondin, M. R. Lohe, F. M. Wisser, J. Grothe, N. Mohamed-Noriega, A. Leifert, S. Dörfler, A. Bachmatiuk, M. H. Rümmeli, S. Kaskel, Electroless copper deposition on (3-mercaptopropyl)triethoxysilane-coated silica and alumina nanoparticles, Electrochim. Acta 114 (2013) 521-526.

[35] Y. Wang, S. Luo, K. Ren, S. Zhao, Z. Chen, W. Li, J. Guan, Facile preparation of graphite particles fully coated with thin Ag shell layers for high performance conducting and electromagnetic shielding composite materials, J. Mater. Chem. C 4 (2016) 2566-2578.

[36] S. Zhou, X. Zhou, G. Hao, W. Jiang, T. Wang, Property control of graphene aerogels by in situ growth of silicone polymer, Appl. Surf. Sci. 439 (2018) 946-953.

[37] R. Hesse, T. Chassé, R. Szargan, J. A. Fresenius, Peak shape analysis of core level photoelectron spectra using

UNIFIT for WINDOWS, Fresenius J. Anal. Chem. 365 (1999) 38-54.

[38] D. A. Shirley, High-Resolution X-Ray Photoemission Spectrum of the Valence Bands of Gold, Phys. Rev. B, 5 (1972) 4709-4715.

[39] F. Kayaci, S. Vempati, I. Donmez, N. Biyikli, T- Uyar, Role of zinc interstisials and oxygen vacancies of ZnO in photocatalysis: a bottom-up approach to control defect density, Nanascale 6 (2014) 10224-10234.

[40] Duchoslav, R. Steinberger, M. Arndt, D. Stifter, XPS study of zinc hydroxide as a potential corrosion product of zinc: Rapid X-ray induced conversion into zinc oxide, Corros. Sci. 82 (2014) 356-361.

[41] A. Sandmann, A. Kompch, V. Mackert, C. H. Liebscher, M. Winterer, Interaction of L-cysteine with ZnO: structure, surface chemistry and optical properties, Langmuir 31 (2015) 5701-5711.

[42] Y. He, L. Wang, L. Zhang, M. Li, X. Shang, Y. Fang, C. Chen, Solubility limits and phase structures in epitaxial ZnOS alloy films grown by pulsed laser deposition, J. Alloys Comp. 534 (2012) 81-85.

[43] G. Wang, Z. Li, M. Li, C. Chen, S. Lv, J. Liao, Aqueous Phase Synthesis and Enhanced Field Emission Properties of ZnO-Sulfide Heterojunction Nanowires, Sci. Rep. 6 (2016) 29470.

[44] P. Banerjee, P. K. Jain, Mechanism of sulfidation of small zinc oxide nanoparticles, RSC Adv. 8 (2018) 34476-34482.

[45] A. Di Mauro, M. Cantarella, G. Nicotra, V. Privitera, Low temperature atomic layer deposition of ZnO: Applications in photocatalysis, Appl. Catal. B: Environ. 196 (2016) 68-76.

[46] H. Frankenstein, C. Z. Leng, M. D. Losego, G. L. Frey, Atomic layer deposition of ZnO electron transporting layers directly onto the active layer of organic solar cells, Org. Electron. 64 (2019) 37-46.

[47] R. G. Wilson, F. A. Stevie, C. W. Maggee (Eds.), Secondary Ion Mass Spectroscopy. A Practical Handbook for Depth Profiling and Bulk Impurity Analysis, New York: John Wiley & Sons, Inc., 1989.

[48] Y. Wang, J. Wen, S. Zhao, Z. Chen, K Ren, J Sun, J. Guan, Surface Thiolation of Al Microspheres to Deposite Thin and Compact Ag Shells for High Conductivity, Langmuir 31 (2015) 13441-13451.

[49] Y.-Q. Cao, J. Chen, H. Zhou, L. Zhu, X. Li, Z.-Y. Cao, D. Wu, A.-D. Li, Photocatalytic activity and photocorrosion of atomic layer deposited ZnO ultrathin films for the degradation of methylene blue, Nanotechnology 26 (2015) 024002.

[50] C.-M. Wu, J. Baltrusaitis, E. G. Gillan, V. H. Grassian, Sulfur Dioxide Adsorption on ZnO Nanoparticles Nanorods, J. Phys. Chem. C 115 (2011) 10164-10172.

[51] G. J. Kluth, M. M. Sung, R. Maboudian, Thermal Behavior of Alkylsiloxane Self-Assembled Monolayers on the Oxidized Si(100) Surface, Langmuir 13 (1997) 3775-3780.

[52] W. Wang, G. Tian, L. Zong, Q. Wang, Y. Zhou, A. Wang, Mesoporous hybrid Zn-silicate derived from red palygorkite clay as a high-efficient adsorbent for antibiotics, Micropor. Mesopor. Mat. 234 (2016) 317-325.

[53] V. Rogé, N. Bahlawane, G. Lamblin, I. Fechete, F. Garin, A. Dinia, D. Lenoble, Improvement of the photocatalytic degradation property of atomic layer deposited ZnO thin films: the interplay between film properties and functional performances, J. Mater. Chem. A 3 (2015) 11453-11461.

[54] K.-H. Park, G. D. Han, B. J. Kim, E. H. Kang, J. S. Park, J. H. Shim, H.-D. Park, Effects of atomic layer deposition conditions on the formation of thin ZnO films and their photocatalytic characteristics, Ceram. Int. 45 (2019) 18823-18830.

[55] D. F. Ollis, Kinetics of Photocatalyzed Reactions: Five Lessons Learned, Front. Chem. 6 (2018) 378.

[56] D. Wawrzynczyk, B. Cichy, W. Stek, M. Nyk, The role of L-cysteine and introduced surface defects in reactive oxygen species generation by ZnO nanoparticles, Dalton Trans., 47 (2018) 8320-8329.

[57] S. Liao, H. Donggen, D. Yu, Y. Su, G. Yuan, Preparation and characterization of ZnO/TiO_2, $SO4^{2-}/ZnO/TiO_2$ photocatalyst and their photocatalysis, J. Photoche. Photobiol. A 168 (2004) 7-13.

[58] D. M. King, X. Liang, B. B. Burton, M. K. Akhtar, A. W. Weimer, Passivation of pigment-grade TiO_2 particles by nanothick atomic layer deposited SiO_2 films, Nanotechnology 19 (2008) 255604.